# Role of boron diffusion in CoFeB/MgO magnetic tunnel junctions

Sumanta Mukherjee,[1] Ronny Knut,[2] S. M. Mohseni,[3,4] T. N. Anh Nguyen,[3,5] S. Chung,[3] Q. Tuan Le,[3] Johan Åkerman,[3,6] Johan Persson,[3] Anindita Sahoo,[1,7] Abhijit Hazarika,[1] Banabir Pal,[1] Sebastian Thiess,[8] Mihaela Gorgoi,[9] P. S. Anil Kumar,[7] Wolfgang Drube,[8] Olof Karis,[2] and D. D. Sarma[1,2,10,*]

[1]*Solid State and Structural Chemistry Unit, Indian Institute of Science, Bangalore 560012, India*
[2]*Department of Physics and Astronomy, Box 516, 75120 Uppsala, Sweden*
[3]*Materials Physics, School of ICT, KTH Royal Institute of Technology, Electrum 229, 164 40 Kista, Sweden*
[4]*Department of Physics, Shahid Beheshti University, Evin, Tehran 19839, Iran*
[5]*Spintronics Research Group, Laboratory for Nanotechnology (LNT), VNU-HCM, Ho Chi Minh City, Vietnam*
[6]*Department of Physics, University of Gothenburg, Gothenburg, Sweden*
[7]*Department of Physics, Indian Institute of Science, Bangalore 560012, India*
[8]*Deutsches Elektronen-Synchrotron DESY, Notkestrasse 85, D-22607 Hamburg, Germany*
[9]*Helmholtz Zentrum Berlin für Materialien und Energie GmbH, Albert Einstein Straße 15, 12489 Berlin, Germany*
[10]*Council of Scientific and Industrial Research–Network of Institutes for Solar Energy (CSIR-NISE), New Delhi 110001, India*

(Received 20 March 2014; revised manuscript received 31 December 2014; published 27 February 2015)

Several scientific issues concerning the latest generation read heads for magnetic storage devices, based on CoFeB/MgO/CoFeB magnetic tunnel junctions (MTJs) are known to be controversial, including such fundamental questions as to the behavior and the role of B in optimizing the physical properties of these devices. Quantitatively establishing the internal structures of several such devices with different annealing conditions using hard x-ray photoelectron spectroscopy, we resolve these controversies and establish that the B diffusion is controlled by the capping Ta layer, though Ta is physically separated from the layer with B by several nanometers. While explaining this unusual phenomenon, we also provide insight into why the tunneling magnetoresistance (TMR) is optimized at an intermediate annealing temperature, relating it to B diffusion, coupled with our studies based on x-ray diffraction and magnetic studies.

DOI: 10.1103/PhysRevB.91.085311 PACS number(s): 73.40.Gk, 79.60.−i, 85.70.Kh

## I. INTRODUCTION

Magnetic tunnel junctions (MTJs) are of great importance due to their application in spin-transfer torque-based devices, e.g., magnetic random access memory (MRAM), high-frequency microwave sources, and in magnetic sensors [1–6]. Presently, sensors used in modern disk drives rely on tunnel magnetoresistance (TMR) in trilayer CoFeB/MgO/CoFeB structures, which succeeds earlier generation devices based on CoFe [4,7]. While device fabrication has been empirically refined to meet strict quality demands, the fundamental understanding of the modifications in the TMR structure introduced by various optimization processes, e.g., postannealing [8–16], resulting in a different magnitude of the TMR [10,11], is still missing. In particular, the behavior of boron, apparently playing a crucial role for high magnetoresistance, has remained controversial in spite of extensive investigations [12,13,15–24]. For example, it has been suggested that B diffusion is integral to the creation of a textured CoFe alloy and consequently, high TMR. Many studies claim that boron diffuses into the MgO tunnel barrier [12,13,15,18,19,21–23,25], where its presence is suggested to be detrimental [23,24] to high TMR due to symmetry breaking of the barrier. Some reports, however, relate the improved TMR to diffusion of B into MgO [18,22,26]. For example, theoretical studies have suggested that the band structure of MgO-B also can provide a route for coherent tunneling of electrons and the diffusion of boron may even be beneficial for the TMR in the device [26]. Other reports [16,20] claim that B rather migrates away from MgO, into the cap layer of Ta, resulting in TaB favoring high TMR [16,17]. Thus, while great steps have been made toward improving device performances substantially, there are significant gaps in our understanding of these device structures. We have used hard x-ray photoelectron spectroscopy (HAXPES) [27–31] to investigate a series of TMR structures. HAXPES studies performed with photon energies even in excess of 10 keV allows the probing depth to reach 50 nm or more. This allows the investigation of the electronic structure of buried interfaces [16,21,27–31] and enables an element-specific characterization of modifications of the interface structure with unsurpassed detail. By systematically studying the modifications of the chemical state of the constituents of the device for different structures and postannealing conditions, we are able to provide a detailed geometric interpretation of how elements diffuse and modify the structure. The HAXPES measurements are complemented by x-ray diffraction (XRD) and magnetic measurements to derive a complete understanding of all aspects controlling physical properties of these samples.

## II. EXPERIMENT

We have used three sets of samples: (i) a complete trilayer structure with a protective Ta cap on top Ta(5)/Ru(10)/Ta(5)/CoFeB(5)/MgO(2)/CoFeB(1)/Ta(5) (sample T); (ii) a bilayer of the form Ta(5)/Ru(10)/Ta(5)/CoFeB(5)/MgO(2) (sample B-1); and (iii) a bilayer with Ta capping on top of the MgO, namely, Ta(5)/Ru(10)/Ta(5)/CoFeB(3)/MgO(1)/Ta(1.8) (sample B-2). The composition of the CoFeB layers was

*Also at Jawaharlal Nehru Centre for Advanced Scientific Research, Bangalore 560064, India; sarma@sscu.iisc.ernet.in

 

$Co_{20}Fe_{60}B_{20}$ and the numbers in parentheses refer to layer thicknesses in nanometers. The samples were grown by means of dc and rf magnetron sputtering. The base pressure in the sputter system was $1.0 \times 10^{-8}$ Torr. The Ta and the MgO layers were rf sputtered at 2.5 and 1.5 mTorr, respectively. The CoFeB electrodes were dc sputtered at 5 mTorr. Optimum Ta smoothness as a function of pressure was established by means of low-angle x-ray reflectivity. MTJ structures grown under the same conditions but with the same thickness of the top and bottom ferromagnetic CoFeB layers (5 nm) were characterized for their TMR as a function of postannealing temperature. We find the maximum TMR value averaged over the whole wafer to be around 100% for the 300 °C-annealed sample. (See the Results and Discussion section.) HAXPES experiments were performed at the HIKE experimental station at the KMC-1 bending magnet beamline [29] in BESSY II, HZB, Berlin and at the HAXPES end station at the undulator beamline P09 [30] of PETRA-III, DESY, Hamburg, Germany. Core-level spectra (Co $2p$, Fe $2p$, B $1s$, Mg $1s$, O $1s$, Ta $4f$) were collected at different photon energies using a fixed, grazing incidence geometry (∼7 degrees grazing incidence). Spectra were obtained for both the as-grown samples and after *in situ* annealing for 20 min in subsequent steps at the following temperatures: $300 \pm 5$ °C, $420 \pm 10$ °C, and $520 \pm 10$ °C at a base pressure of $10^{-9}$ Torr. Structural parameters were determined using an already established protocol based on photoelectron spectroscopy [32–35].

## III. RESULTS AND DISCUSSION

Normalized HAXPES spectra collected for Fe $2p$ and B $1s$ at different photon energies between 3000 and 5000 eV from sample T, representative of an actual TMR device structure, are shown in Figs. 1(a) and 1(b), after subtracting a Shirley-type background [36]. The spin-orbit split $2p$ peaks of metallic Fe [12,16,21] can be seen [Fig. 1(a)] at binding energies (BEs) of 706.8 and 720.0 eV. The peak corresponding to metallic boron is found at a BE of 187.8 eV, along with a broad, low-intensity feature at ∼192.7 eV, due to various B-oxide species [12,18,20,21]. This suggests a slight oxidation of the CoFeB layer during the growth of MgO, which was accounted for in our analysis. A comparison of the Fe $2p$ and B $1s$ spectra, before and after annealing *in situ* at the optimal ∼300 °C, recorded using 4000 eV photon energy, is given in Figs. 1(c) and 1(d). In contrast to many earlier reports [12,18,21], this comparison makes it clear that we do not observe any change in position or shape of the Fe $2p$ [Fig. 1(c)], B $1s$ [Fig. 1(d)], or in any of the other core-level spectra (not shown). These observations are not specific to any particular excitation energy, giving the same conclusions when we compare the spectra obtained at other photon energies from this annealed sample [inset of Figs. 1(c) and 1(d)] with that of the unannealed sample. The spectral intensity ratios measured at different excitation energies for both the unannealed (circles) and the sample annealed at 300 °C (diamonds) are shown in Fig. 2(a). The intensity ratios between different core levels are almost identical for both the unannealed and the annealed samples. Our data thus clearly suggest that there is no significant diffusion of any of the elements comprising these TMR structures upon annealing at 300 °C, which is the temperature that we find optimizes TMR in our samples. The average TMR over the whole wafer and the resistance area product (RA) obtained from the as-grown and annealed samples are given in Fig. 2(b).

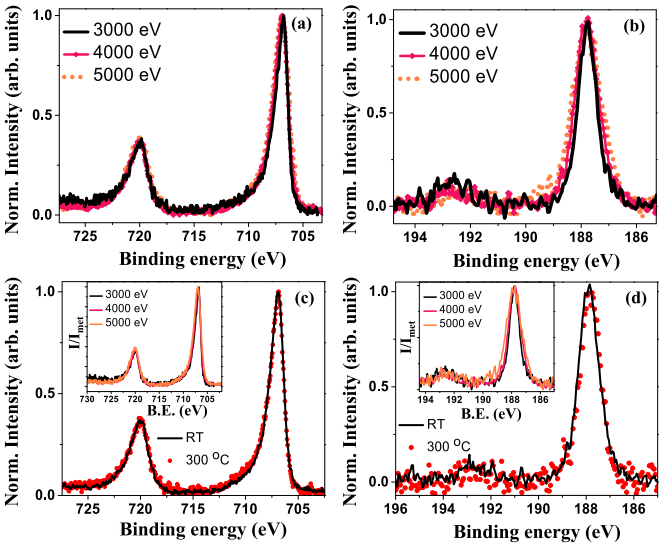


FIG. 1. (Color online) Normalized photoelectron spectra of (a) Fe $2p$ and (b) B $1s$ collected from the as-grown trilayer MTJ sample T at photon energies ranging from 3000 to 5000 eV. Panels (c) and (d) show comparisons of Fe $2p$ and B $1s$ spectra obtained at 4000 eV photon energy from the as-grown (black line) and 300 °C-annealed (red dots) samples. Photon energy dependencies of normalized photoelectron spectra of Fe $2p$ and B $1s$ collected from the 300 °C-annealed sample T are shown in the insets of panels (c) and (d), respectively.

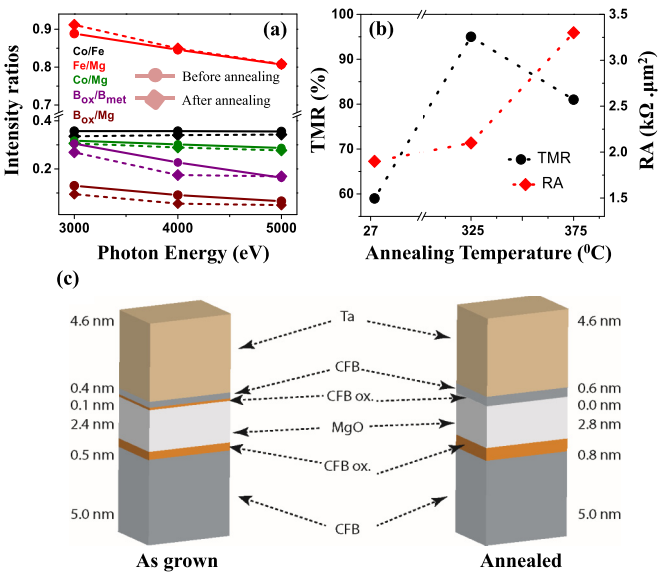


FIG. 2. (Color online) (a) Intensity ratios between different core-level photoelectron spectra obtained at different photon energies from the trilayer sample T, before (circles) and after (diamonds) annealing the sample at 300 °C. (b) The average TMR (averaged over the whole wafer) and the resistance area product (RA) obtained from sample T under different annealing conditions. (c) The thickness and nature of various layers in the capped trilayer sample T, as deduced from the analysis of core-level intensities as a function of the photon energy.

We have followed the procedure described in Refs. [32–35] to obtain quantitative information on the layer stacking and thicknesses, using the spectral intensity ratios measured at different excitation energies.

Briefly, in this method the differential intensity contribution to a core-level photoelectron spectrum of a particular atom contained in a volume element $dV$ of the sample at a depth $z$ from the surface of the sample can be expressed as

$$dI = n\sigma I_0 \exp(-z/\lambda \cos\theta) dV, \quad (1)$$

where $\lambda$ is the mean free path of the photoelectron, $\sigma$ is the photoionization cross section of that particular core-level spectra, and the constant $I_0$ comes from the experimental condition and depends on instrument geometry, photon flux, transmission function, and angle of acceptance of the analyzer. $\theta$ is the photoelectron emission angle and $n$ is the number density of that particular element within the volume element $dV$. The total photoemission spectral intensity of that particular core level can then be estimated by integrating Eq. (1) over the whole volume of the sample. For the present thin-film geometry the total photoemission intensity can be expressed as

$$I = \int_v dI = \sigma I_0 \int_0^z n(z) \exp(-z/\lambda \cos\theta) dz. \quad (2)$$

For a thin-film system containing an element $A$ down to a depth of $z_1$ and element $B$ from a depth of $z_1$ to $z_2$, the intensity ratios at different photon energies can be expressed as

$$\frac{I_A(h\nu)}{I_B(h\nu)} = \frac{\int_v dI_A(h\nu)}{\int_v dI_B(h\nu)} = \frac{\sigma_A(h\nu)}{\sigma_B(h\nu)} \frac{\int_0^{z_2} n_A(z) \exp[-z/\{\lambda_A(h\nu)\cos\theta\}] dz}{\int_0^{z_2} n_B(z) \exp[-z/\{\lambda_B(h\nu)\cos\theta\}] dz}, \quad (3)$$

where $n(z)$ is the number density of a particular element which depends only on the depth $z$ for a laterally homogeneous and planar structure, which is the model structure assumed for our samples. For example, $n(z)$ will have the following form for a model structure with an atomically sharp interface between $A$ and $B$, $n_A(z)$ and $n_B(z)$, having the following forms:

$$n_A(z) = n_A \quad \text{for} \quad 0 \leqslant z \leqslant z_1$$
$$= 0 \quad \text{for} \quad z_1 \leqslant z \leqslant z_2,$$

$$n_B(z) = 0 \quad \text{for} \quad 0 \leqslant z \leqslant z_1$$
$$= n_B \quad \text{for} \quad z_1 \leqslant z \leqslant z_2.$$

Including the values of $n(z)$ in Eq. (3) in this case, we obtain the equation for the intensity ratio as

$$\frac{I_A(h\nu)}{I_B(h\nu)} = \frac{\int_v dI_A(h\nu)}{\int_v dI_B(h\nu)} = \frac{\sigma_A(h\nu)}{\sigma_B(h\nu)} \frac{\int_0^{z_1} n_A \exp[-z/\{\lambda_A(h\nu)\cos\theta\}] dz}{\int_{z_1}^{z_2} n_B \exp[-z/\{\lambda_B(h\nu)\cos\theta\}] dz}. \quad (4)$$

Thicknesses $z_1$ and $z_2$, defining the model used in this example, can be obtained by using Eq. (4) to fit the experimentally obtained intensity at a number of different photon energies within a least-squared-error approach.

It can be easily seen that this quantitative estimation of the internal structure is not only restricted to sharp interfaces, since different kinds of structure can be modeled by proper choices of the parameter $n(z)$ to get the best fitting of the experimental intensity ratio. We have fitted the intensity ratios obtained from the photoelectron spectra of sample T [Fig. 2(b)] and out of many modeled structures considered, the best fits to all the intensity ratios were obtained for the structures shown in Fig. 2(c) for sample T before and after annealing at 300 °C. To make our estimates of the thicknesses (tunnel barrier and interdiffused regions) less uncertain, we kept the thicknesses of the top Ta and the lower CoFeB layers to be 4.6 and 5.0 nm and the composition of the CoFeB layers as $Co_{20}Fe_{60}B_{20}$. The estimated errors in thicknesses of the MgO and top CoFeB layers are ±0.4 and ±0.1 nm, respectively. We also need a very thin (<1nm) oxide layer [Fig. 2(c)] between the CFB and MgO layers to simulate the intensity ratios properly. As evident from Fig. 2(c), we observe basically no change between the structures of the as-grown and 300 °C-annealed sample.

These results directly contradict a large number of results in the literature reporting diffusion of boron into MgO at 300 °C [12,13,15,18,19,21,25]. However, there are a few reports in the literature [16,17] that are in apparent agreement with our results. These contradictory results from samples that are apparently made the same way prompted us to scrutinize published data carefully. This revealed a systematic trend that experiments carried out on samples without a protective cap (for example Ta) show diffusion of boron into MgO [12,13,15,21], whereas studies performed on samples with a protective layer do not [16]. This generalization appears almost always to be in agreement with published results so far, though not identified by anyone; our present results on samples with Ta capping in Figs. 1 and 2(c) are also consistent with this trend. To test this hypothesis, we carried out further studies on a bilayer MTJ sample without Ta cap (sample B-1) as well as on a Ta-capped (sample B-2) bilayer samples. The consequence of capping is clearly seen in the spectra of Fe $2p$ and B $1s$ shown in Figs. 3(a)–3(d) for both samples. The spectra collected from the as-deposited uncapped sample B-1 [Figs. 3(a) and 3(b)] are noticeably different from the capped trilayer sample, and the annealing strongly influences the core-level spectra and hence the chemical structure of the layer stack. For example, the boron oxide content is higher in this sample, and the oxidation of Fe is also evident in the Fe $2p$ spectrum. Upon annealing, the B $1s$ oxide species is found to increase markedly at the expense of the B $1s$ metallic peak intensity, whereas for Fe $2p$ the intensity of the metallic peak increases at the expense of the oxide intensity. The Co $2p$ spectrum (not shown) with an evidence of partial oxidation behaves similar to Fe $2p$. Additionally, the relative intensity of the B oxide signal compared to the B metal signal is invariably found to decrease with an increasing photon energy, while it was found to alter slightly with respect to the Mg signal, as illustrated for the annealed B-1 sample in the inset to Fig. 3(a). These observations are readily attributed to the diffusion of boron into MgO, as also suggested in the literature [12,18,21]. Our quantitative analysis of the intensity ratio reveals the internal structure of the uncapped bilayer sample B-1 before and after annealing, as shown in Figs. 3(e) and 3(f). The as-deposited sample shows the presence of a thin B-oxide layer

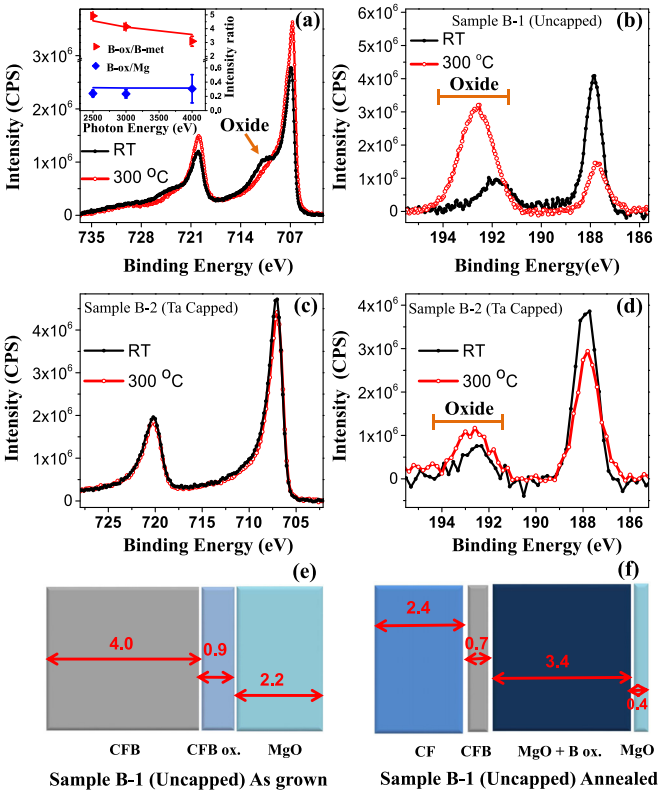


FIG. 3. (Color online) (a, b) Fe 2$p$ and B 1$s$ core-level spectra collected from the uncapped bilayer sample B1 at 3000 eV photon energy before (black) and after (red) annealing the sample at $300 \pm 5\,^{\circ}$C for 20 min. (c, d) The same spectra for the Ta-capped bilayer sample B2 collected at 3600 eV. The inset of (a) shows the intensity ratio between B oxide to B metal (red triangles) and B oxide to Mg (blue square) obtained from the $300 \pm 5\,^{\circ}$C annealed sample B1 at different photon energies. The lines represent the intensity ratios for the best fitted structure, shown in (f). The thickness and nature of various layers in the unannealed and annealed uncapped bilayer sample B1 are shown in (e) and (f). The numbers shown in the figures are in nanometers.

($0.9 \pm 0.1$ nm) at the interface between the MgO ($2.2 \pm 0.2$ nm) and CoFeB ($4.0 \pm 0.3$ nm) layers [Fig. 3(e)]. Upon annealing, B diffuses out from the CoFeB and forms a thick ($3.4 \pm 0.2$ nm) mixed layer of MgO and B oxide [$(1 - x)$MgO + ($x$) B oxide; $x = 0.4$], sandwiched between the MgO ($0.4 \pm 0.1$ nm) and CoFeB ($0.7 \pm 0.1$ nm) layers. Such diffusion of B from the CoFeB matrix results in formation of a CoFe-rich layer ($2.4 \pm 0.2$ nm) towards the bottom of the CoFeB layer [Fig. 3(f)].

Corresponding results for the sample with the protective Ta cap (B-2) [Figs. 3(c) and 3(d)] show an almost complete suppression of the above-mentioned effects. The Fe 2$p$ spectrum [Fig. 3(c)] of the as-prepared sample is essentially free of any oxide signal and is unaffected by annealing, where the formation of boron oxide is largely suppressed [Fig. 3(d)] compared to the uncapped sample [Fig. 3(b)]. The intensity ratios of various core levels obtained from the Ta-capped bilayer sample were found to vary only slightly upon annealing, suggesting a very effective suppression of B migration upon capping, even for this bilayer sample. Thus, these results clearly establish a direct correlation between the B diffusion and oxidation in absence of a cap and a near-complete absence of such migration of B in presence of a Ta cap layer, irrespective of the sample being bi- or a trilayer. These results rationalize all the contradictory reports existing in the literature. The observation of the behavior of B being fundamentally altered by a layer of Ta, which is physically separated from the boron-containing CFB layer by a several-nanometers-thick layer of MgO, may be understood as follows. The diffusion of B towards MgO, for example, in the uncapped bilayer sample, is driven by the energy lowering associated with the oxidation of B. However, B cannot reduce stoichiometric MgO for energetic reasons. The only way B may be oxidized is by the presence of excess oxygen in the structure or by transportation towards the surface. It is important to note that we find evidence of extensive formation of carbonate species due to the reaction of the uncapped MgO with $CO_2$. Such carbonates on top of MgO act as a source of oxygen for B to oxidize, with B diffusing through MgO and an associated diffusion of oxygen ions towards the CFB layer, as described within the Mott-Cabrera theory of oxidation [37]. Thus, the B diffusion and oxidation, as well as the conversion of the carbonate on the MgO surface to MgO, must all go together, driven by the same chemical potential. We indeed find evidence of modifications of surface carbonate species with the oxidation and migration of B in the uncapped sample upon annealing. By capping the top surface with Ta, we cut off the oxygen source, which is essential for the oxidation and diffusion of B.

Few studies [16] report migration of B towards the opposite Ta layer instead of towards the MgO layer. These experiments are typically carried out on samples annealed at higher temperatures ($>500\,^{\circ}$C). To gain further insights on the impact of high-temperature annealing, we have carried out HAXPES experiments with stepwise annealing of the sample T up to $520\,^{\circ}$C under UHV conditions. Figures 4(a) and 4(b) show spectra of Fe 2$p$ and B 1$s$ core levels of sample T recorded at 4000 eV excitation energy and the effect of high-temperature annealing. It is clearly seen [Fig. 4(b)] that the intensity of the B-oxide peak increases with respect to the metallic B 1$s$ peak at higher annealing temperature, though the effect is much less pronounced compared to the uncapped B-1 sample. Changes are also found in the Fe 2$p$ spectra, where the intensity at 709.9 eV BE, corresponding to the binding energy of Fe oxide [12,18,21], is depleted upon annealing. These observations suggest that the more electropositive B oxidizes itself by reducing the thin oxide layer of CoFe at the interface of CoFeB and MgO [see Fig. 2(c)]. This makes a part of the B present in the CFB layers move towards the MgO layer. With additional measurements at a high photon energy of 8000 eV, to make the lower Ta/CFB interface visible, we also observed the formation of TaB, suggesting boron diffusion towards the lower interface at high annealing temperatures, in agreement with other studies [16]. There are several possible consequences of our findings concerning boron diffusion. Diffusion of B into MgO can create pinholes in the MgO lattice [23], leading to leakage and decreased TMR. It can also alter the symmetry of the MgO lattice [24], again leading to a decreased TMR. It has furthermore been proposed that small amounts of Fe oxide at the interface of CFB can improve the TMR significantly [22,38]. The reduction of

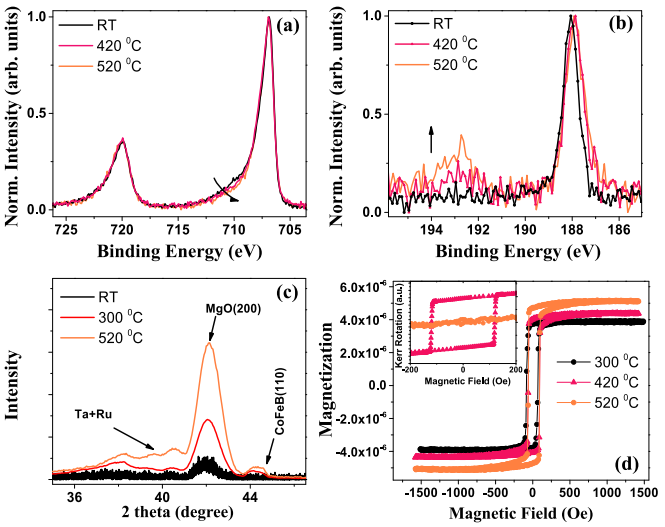


FIG. 4. (Color online) Comparison of Fe $2p$ (a) and B $1s$ (b) spectra, collected for trilayer sample T at 4000 eV photon energy before and after annealing the sample *in situ* at 420 °C for 20 min and subsequently to 520 °C for 20 min. (c, d) The effect of annealing on the x-ray diffraction pattern and on the magnetization, respectively. The inset in panel (d) shows that the perpendicular anisotropy is removed upon annealing at high annealing temperature.

such interface oxide should therefore have a negative effect on the TMR. Considering the conditions for optimal TMR in our samples, with the results obtained from HAXPES, we arrive at the conclusion that the optimal annealing temperature for TMR is the maximum temperature where boron diffusion is still avoided. We have also looked into the effect of annealing on other physical properties of the TMR device, e.g., crystallinity and magnetic behavior, which plays an important roles in determining the TMR. For the as-deposited sample the MgO(200) peak [10,15] is very broad and weak [Fig. 4(c)], signifying the amorphous nature of the as-grown sample. Annealing to 300 °C appears sufficient to crystallize the MgO layer. Higher-temperature annealing does not change the FWHM of the MgO(200) peak significantly. The CFB peak, on the other hand, has very low intensity, making a detailed analysis based on the temperature dependence of the diffraction from CFB difficult. To obtain independent information on physical properties of the CFB layers, we therefore performed Magneto-optical Kerr Effect (MOKE) and magnetization measurements. Our magnetization data [Fig. 4(d)] suggest that the sample annealed at 300 °C already has strong in-plane magnetization and increases only slightly with an increasing annealing temperature. We conclude that annealing to higher temperatures does not lead to substantial improvements of the crystallinity of the MgO layer or of the magnetic properties of the CFB. Interestingly, there is a finite perpendicular magnetic anisotropy (PMA) present in all the samples, which completely vanishes at 520 °C annealing, as shown by the polar MOKE data in the inset of Fig. 4(d). Such a removal of perpendicular anisotropy could possibly lead to a decrease in the TMR value [14]. The depletion of Fe/Co oxide at the interface and the reduction of the PMA suggest a correlation between PMA and the existence of interfacial oxides. Theoretically it has been suggested that the PMA found in CFB/MgO/CFB structures is driven by hybridization to oxygen at the CFB/MgO interface [39]. Our observation principally supports this conclusion. However, our data suggest that the interfacial contribution to the PMA is due to the existence of a few angstroms thick, partially oxidized CFB layer. This thin layer is reduced by boron when boron starts to diffuse into the MgO layer upon annealing at a relatively high temperature. This suggests a very delicate balance of the stoichiometry of the interface to stabilize a PMA in CFB/MgO/CFB tunnel junctions.

## IV. CONCLUSION

In conclusion, we have achieved quantitative descriptions of the internal structure of magnetic tunnel junctions annealed at various temperatures using hard x-ray photoelectron spectroscopy. Our data provides a resolution to apparently conflicting claims concerning B diffusion at moderate annealing temperatures. Our results establish that boron does not diffuse beyond one or two atomic planes at the interface of CoFeB and MgO under conditions typical for device fabrication, in a pristine well-capped trilayer sample. Higher temperature annealing allows a small fraction of boron to move into MgO, reducing Fe and Co oxides present at the interface and forming B oxide. We have found indications that this reduction is detrimental to any perpendicular magnetic anisotropy in the system. These results indicate that 300 °C annealing is sufficient for the crystallization of MgO and magnetization of the CoFeB layer in our samples.

## ACKNOWLEDGMENTS

We thank the Department of Science and Technology, Ministry of Science and Technology, India and the Swedish Foundation for International Cooperation in Research and Higher Education for financial support.

[1] J. Åkerman, Science **308**, 508 (2005).
[2] A. M. Deac, A. Fukushima, H. Kubota, H. Maehara, Y. Suzuki, S. Yuasa, Y. Nagamine, K. Tsunekawa, D. D. Djayaprawira, and N. Watanabe, Nat. Phys. **4**, 803 (2008).
[3] S. A. Wolf, D. D. Awschalom, R. A. Buhrman, J. M. Daughton, S. von Molnár, M. L. Roukes, A. Y. Chtchelkanova, and D. M. Treger, Science **294**, 1488 (2001).
[4] S. S. P. Parkin, C. Kaiser, A. Panchula, P. M. Rice, B. Hughes, M. Samant, and S. Yang, Nat. Mater. **3**, 862 (2004).
[5] S. Yuasa, T. Nagahama, A. Fukushima, Y. Suzuki, and K. Ando, Nat. Mater. **3**, 868 (2004).
[6] S. Ikeda, K. Miura, H. Yamamoto, K. Mizunuma, H. D. Gan, M. Endo, S. Kanai, J. Hayakawa, F. Matsukura, and H. Ohno, Nat. Mater. **9**, 721 (2010).

[7] F. Bonell, T. Hauet, S. Andrieu, F. Bertran, P. Le Fèvre, L. Calmels, A. Tejeda, F. Montaigne, B. Warot-Fonrose, B. Belhadji, A. Nicolaou, and A. Taleb-Ibrahimi, Phys. Rev. Lett. **108**, 176602 (2012).
[8] D. D. Djayaprawira, K. Tsunekawa, M. Nagai, H. Maehara, S. Yamagata, N. Watanabe, S. Yuasa, Y. Suzuki, and K. Ando, Appl. Phys. Lett. **86**, 092502 (2005).
[9] W. G. Wang, J. Jordan-Sweet, G. X. Miao, C. Ni, A. K. Rumaiz, L. R. Shah, X. Fan, P. Parsons, R. Stearrett, E. R. Nowak, J. S. Moodera, and J. Q. Xiao, Appl. Phys. Lett. **95**, 242501 (2009).
[10] C. Park, J.-G. Zhu, M. T. Moneck, Y. Peng, and D. E. Laughlin, J. Appl. Phys. **99**, 08A901 (2006).
[11] J. Hayakawa, S. Ikeda, Y. M. Lee, F. Matsukura, and H. Ohno, Appl. Phys. Lett. **89**, 232510 (2006).
[12] J. C. Read, P. G. Mather, and R. A. Buhrman, Appl. Phys. Lett. **90**, 132503 (2007).
[13] J. J. Cha, J. C. Read, R. A. Buhrman, and D. A. Muller, Appl. Phys. Lett. **91**, 062516 (2007).
[14] W. G. Wang, S. Hageman, M. Li, S. Huang, X. Kou, X. Fan, J. Q. Xiao, and C. L. Chien, Appl. Phys. Lett. **99**, 102502 (2011).
[15] S. S. Mukherjee, F. Bai, D. MacMahon, C. L. Lee, S. K. Gupta, and S. K. Kurinec, J. Appl. Phys. **106**, 033906 (2009).
[16] X. Kozina, S. Ouardi, B. Balke, G. Stryganyuk, G. H. Fecher, C. Felser, S. Ikeda, H. Ohno, and E. Ikenaga, Appl. Phys. Lett. **96**, 072105 (2010).
[17] S. Ikeda, J. Hayakawa, Y. Ashizawa, Y. M. Lee, K. Miura, H. Hasegawa, M. Tsunoda, F. Matsukura, and H. Ohno, Appl. Phys. Lett. **93**, 082508 (2008).
[18] Y. Jang, C. Nam, K. S. Lee, B. K. Cho, Y. J. Cho, K. S. Kim, and K. W. Kim, Appl. Phys. Lett. **91**, 102104 (2007).
[19] S. Pinitsoontorn, A. Cerezo, A. K. Petford-Long, D. Mauri, L. Folks, and M. J. Carey, Appl. Phys. Lett. **93**, 071901 (2008).
[20] H. Kurt, K. Rode, K. Oguz, M. Boese, C. C. Faulkner, and J. M. D. Coey, Appl. Phys. Lett. **96**, 262501 (2010).
[21] A. A. Greer, A. X. Gray, S. Kanai, A. M. Kaiser, S. Ueda, Y. Yamashita, C. Bordel, G. Palsson, N. Maejima, S.-H. Yang, G. Conti, K. Kobayashi, S. Ikeda, F. Matsukura, H. Ohno, C. M. Schneider, J. B. Kortright, F. Hellman, and C. S. Fadley, Appl. Phys. Lett. **101**, 202402 (2012).
[22] Y. Lu, M. Tran, H. Jaffrès, P. Seneor, C. Deranlot, F. Petroff, J.-M. George, B. Lépine, S. Ababou, and G. Jézéquel, Phys. Rev. Lett. **102**, 176801 (2009).
[23] K. Komagaki, M. Hattori, K. Noma, H. Kanai, K. Kobayashi, Y. Uehara, M. Tsunoda, and M. Takahashi, IEEE Trans. Magn. **45**, 3453 (2009).
[24] Z. Bai, L. Shen, Q. Wu, M. Zeng, J. S. Wang, G. Han, and Y. P. Feng, Phys. Rev. B **87**, 014114 (2013).
[25] T. Takeuchi, K. Tsunekawa, Y. S. Choi, Y. Nagamine, D. D. Djayaprawira, A. Genseki, Y. Hoshi, and Y. Kitamoto, Jpn. J. Appl. Phys. **46**, L623 (2007).
[26] D. A. Stewart, Nano Letters **10**, 263 (2010).
[27] S. Granroth, R. Knut, M. Marcellini, G. Andersson, S. Svensson, O. Karis, M. Gorgoi, F. Schäfers, W. Braun, W. Eberhardt, W. Olovsson, E. Holmström, and N. Mårtensson, Phys. Rev. B **80**, 094104 (2009).
[28] S. Granroth, W. Olovsson, E. Holmström, R. Knut, M. Gorgoi, S. Svensson, and O. Karis, J. Electron Spectrosc. Relat. Phenom. **183**, 80 (2011).
[29] M. Gorgoi, S. Svensson, F. Schäfers, G. Öhrwall, M. Mertin, P. Bressler, O. Karis, H. Siegbahn, A. Sandell, H. Rensmo, W. Doherty, C. Jung, W. Braun, and W. Eberhardt, Nucl. Instrum. Methods Phys. Res., Sect. A **601**, 48 (2009).
[30] R. Claessen, M. Sing, M. Paul, G. Berner, A. Wetscherek, A. Müller, and W. Drube, New J. Phys. **11**, 125007 (2009).
[31] S. Mukherjee, A. Hazarika, P. K. Santra, A. L. Abdelhady, M. A. Malik, M. Gorgoi, P. OBrien, O. Karis, and D. D. Sarma, J. Phys. Chem. C **118**, 15534 (2014).
[32] L. Kumar, D. D. Sarma, and S. Krummacher, Appl. Surf. Sci. **32**, 309 (1988).
[33] P. K. Santra, R. Viswanatha, S. M. Daniels, N. L. Pickett, J. M. Smith, P. O'Brien, and D. D. Sarma, J. Am. Chem. Soc. **131**, 470 (2009).
[34] D. D. Sarma, A. Nag, P. K. Santra, A. Kumar, S. Sapra, and P. Mahadevan, J. Phys. Chem. Lett. **1**, 2149 (2010).
[35] D. D. Sarma, P. K. Santra, S. Mukherjee, and A. Nag, Chem. Mater. **25**, 1222 (2013).
[36] D. A. Shirley, Phys. Rev. B **5**, 4709 (1972).
[37] N. Cabrera and N. F. Mott, Rep. Prog. Phys. **12**, 163 (1949).
[38] C. Tusche, H. L. Meyerheim, N. Jedrecy, G. Renaud, A. Ernst, J. Henk, P. Bruno, and J. Kirschner, Phys. Rev. Lett. **95**, 176101 (2005).
[39] H. X. Yang, M. Chshiev, B. Dieny, J. H. Lee, A. Manchon, and K. H. Shin, Phys. Rev. B **84**, 054401 (2011).